INSTITUTE OF PHYSICS PUBLISHING JOURNAL OF PHYSICS B: ATOMIC, MOLECULAR AND OPTICAL PHYSICS

J. Phys. B: At. Mol. Opt. Phys. **35** (2002) 4695–4709 PII: S0953-4075(02)37292-4

Differential cross-sections for the electron impact excitation of the B $^1\Sigma_u^+$, c $^3\Pi_u$, a $^3\Sigma_g^+$, C $^1\Pi_u$, E, F $^1\Sigma_g^+$ and e $^3\Sigma_u^+$ states of molecular hydrogen

J Wrkich[1], D Mathews[1], I Kanik[2], S Trajmar[2] and M A Khakoo[1]

[1] Department of Physics, California State University, Fullerton, CA 92834, USA
[2] Jet Propulsion Laboratory, Caltech, Pasadena, CA 91109, USA

Received 21 May 2002, in final form 30 September 2002
Published 6 November 2002
Online at stacks.iop.org/JPhysB/35/4695

Abstract

Using energy loss spectroscopy, normalized differential and integral cross-sections for the electron impact excitation of the lowest bound excited states of H_2 from the ground X $^1\Sigma_g^+$ state have been measured at 17.5, 20 and 30 eV impact energies and for scattering angles from 5° up to 130°. These differential cross-sections (DCSs) are an effort to improve those taken previously (Khakoo M A and Trajmar S 1986b *Phys. Rev.* A **34** 146). Here a more sophisticated electron spectrometer and a more accurate spectrum analysis code is used to unfold the energy loss spectra. The results are compared with earlier DCS measurements for the B $^1\Sigma_u^+$, c $^3\Pi_u$, a $^3\Sigma_g^+$, C $^1\Pi_u$ states of H_2 and with existing theoretical results for the B $^1\Sigma_u^+$, c $^3\Pi_u$, a $^3\Sigma_g^+$, C $^1\Pi_u$, E, F $^1\Sigma_g^+$ and e $^3\Sigma_u^+$ states.

1. Introduction

Despite its importance in ionized plasmas, planetary atmospheres (pollution), astrophysical phenomena and laser systems there has been little work undertaken on the differential electron impact excitation of the low-lying bound states of simple diatomic molecules (e.g. H_2, N_2, O_2, CO, NO) from their respective ground states. There should be a special interest in H_2 because, also, of the intensity of V/FUV emissions from these bound states. The B $^1\Sigma_u^+$, C $^1\Pi_u \rightarrow$ X $^1\Sigma_g^+$ FUV emissions and VUV from the c $^3\Pi_u$, a $^3\Sigma_g^+ \rightarrow$ b $^3\Sigma_u^+$ are notable because they arise abundantly from interstellar media and from planetary atmospheres (especially Jupiter). They have also been observed almost continuously throughout the duration of the space programme, e.g. by the Voyager I and II spacecraft in the early 1980s, the Galileo spacecraft and the Hubble telescope in the 1990s and continuing. There has been some action to model these emissions (see Shemansky *et al* 1985), but this has been restrained by a paucity of experimental data to support such modelling studies. Recently, there has been practical need for electron collision data for molecules in such excited states based on developments in plasma reactor work for semiconductor processing undertaken by Pinnaduwage and Christophorou (1993, 1994).

The only measurements taken of the differential electron impact excitation of H_2, for the low-lying bound states, have been those of Srivastava and Jensen (1977) and Khakoo and Trajmar (1986b). The energy loss spectrum of H_2 is complicated by heavily overlapping electronic-vibrational manifolds, which are difficult to unravel. However, with the development of high-resolution energy loss spectrometers and advances in computer technology, it is now possible to systematically unravel (unfold) such spectra. This results in improved quality data in the form of differential cross-sections (DCSs) and enables one to provide a better test of theoretical models. The most common molecular species in the interstellar medium is H_2, which produces strong emissions in the VUV, e.g. in the form of the Lyman and Werner bands. As a significant fraction of such VUV emissions is excited by electron impact, such data are expected to benefit astrophysics research.

Within reason, H_2 being the simplest molecule, one would expect the situation for electron impact excitation for this molecule (i.e. agreement between experimental and theoretical cross-sections) to be the best of any molecule. However, this is not the case. There is considerable disagreement between experimental and theoretical data and in part this is due to a severe paucity of experimental excitation cross-sections. Several theoretical models have been developed: the initial distorted wave calculations of Rescigno *et al* (1976) (b $^3\Sigma_u^+$ and a $^3\Sigma_g^+$ states), Fliflet and McKoy (1980) (b $^3\Sigma_u^+$ and B $^1\Sigma_u^+$ states) and Mu-Tao *et al* (1982) (C $^1\Pi_u$, c $^3\Pi_u$, B$'$ $^1\Sigma_u^+$ and E, F $^1\Sigma_g^+$ states). These were followed by a multi-channel Schwinger variational calculation of Lima *et al* (1988) (b $^3\Sigma_u^+$, a $^3\Sigma_g^+$, c $^3\Pi_u$ states). Later, Mu-Tao *et al* (1982) also investigated electron correlation effects in their earlier calculations and extended their calculations to other states (b $^3\Sigma_u^+$, a $^3\Sigma_g^+$, c $^3\Pi_u$ states). More recently, Parker *et al* (1991) have carried out a complex Kohn variational method (b $^3\Sigma_u^+$, a $^3\Sigma_g^+$, c $^3\Pi_u$ states) which is a variation of the distorted wave. The *R*-matrix close-coupling method (Burke and Robb 1975) has more recently been applied to excitation of H_2 by Branchett *et al* (1990, 1991) (b $^3\Sigma_u^+$, a $^3\Sigma_g^+$, c $^3\Pi_u$, B $^1\Sigma_u^+$ and E, F $^1\Sigma_g^+$ states). Whereas the *R*-matrix results gave excellent agreement with elastic scattering experimental cross-sections, it did not do as well for inelastic DCSs.

Experimental DCSs for the excitation of H_2 have been those of Weingartshofer *et al* (1970) at low energies (b $^3\Sigma_u^+$ and B $^1\Sigma_u^+$ states), Trajmar *et al* (1968) (b $^3\Sigma_u^+$ state), Hall and Andric (1984) (b $^3\Sigma_u^+$ state), Nishimura and Danjo (1986) (b $^3\Sigma_u^+$ state), Khakoo and Trajmar (1986b) (a $^3\Sigma_g^+$, c $^3\Pi_u$, B $^1\Sigma_u^+$ and C $^1\Pi_u$ states), Khakoo and Trajmar (1987) (b $^3\Sigma_u^+$ state), Srivastava and Jensen (1977) (B $^1\Sigma_u^+$ state) and Khakoo and Segura (1994) (b $^3\Sigma_u^+$ state).

In the present case, we were motivated to improve and extend our earlier measurements (Khakoo and Trajmar 1986b), in particular the method of analysis of the results (unfolding). This was undertaken because of the disagreements between theory and our earlier measurements, which consequently invited further investigation into an improvement of the existing situation from an experimental standpoint. With the availability of a better spectrometer and a more sophisticated data analysis program for molecular spectra, this was deemed feasible and warranted.

2. Method

2.1. Data analysis algorithm and FC factors used

The present DCSs can be expected to be an improvement over the previous DCSs of Khakoo and Trajmar (1986b) for the following reasons.

(i) A double-hemispherical spectrometer (described in Guo *et al* 2000) with a better-characterized instrumental line function was used. This instrument acquires spectra with significantly reduced line-wing profiles compared with those that normally occurred in the single-hemispherical instrument used in the earlier measurements. This enabled us to unfold the spectra without incurring systematic errors due to these line-wings that are difficult to synthesize in unfolding algorithms.

(ii) A more sophisticated multi-Gaussian spectrum unfolding routine was used (see Khakoo and Segura 1994) as compared to the single Gaussian algorithm used in the earlier work of Khakoo and Trajmar (1986b), which was adapted for molecules. In this case the molecular spectrum in terms of intensity $S(E_0, \theta, \Delta E)$ versus energy loss (ΔE), at the fixed incident energy E_0 and scattering angle θ, was fitted to the function (see Khakoo and Trajmar 1986b)

$$S(E_0, \theta, \Delta E) = C \sum_{n'=0}^{N} \sigma_{n'}(E_0, \theta) \sum_{v'=0}^{M(n')} q_{n',v} F_{n',v}(\Delta E - \Delta E_{n',v}) + \boldsymbol{B}(E_0, \theta, \Delta E, \rho, I_0) \quad (1)$$

except that in this case the normalized instrumental line function

$$F_{n',v}(\Delta E - \Delta E_{n',v}) = \sum_{m=1}^{M} \frac{A_m}{\Delta_m \sqrt{\pi}} \exp\left[-\left[\frac{\Delta E - \Delta E_{n',v} - \Delta E_m}{\Delta_m} \right]^2 \right] \quad (2)$$

is a multi-Gaussian function of order M (with each Gaussian located off the line centre by the energy loss amount ΔE_m, relative intensity A_m and width Δ_m). $\Delta E_{n',v}$ is the energy loss value for the v vibrational level for the n' electronic state (see table 1). This function was synthesized from a non-linear least-squares fitting to an isolated feature (e.g. the $B\,^1\Sigma_u^+$ ($v = 2$ or 3) feature) in the spectrum. In equation (1), the $q_{n',v}$ are the Franck–Condon (FC) factors for the vibrational transitions $X\,^1\Sigma_g^+(v'' = 0) \rightarrow n'(v)$ in the electronic manifold n'. The $\sigma_{n'}(E_0, \theta)$ are the DCSs for the excitation of the electronic state n'. C is the normalization constant. The function

$$B(E_0, \theta, \Delta E, \rho, I_0), = \sum_{i=0}^{I<3} \boldsymbol{B}_i \Delta E^i \quad (3)$$

which represented the background was expressed as a polynomial of up to order 2 and was dependent on the incident electron current I_0 and target gas density distribution ρ. In equations (1) and (3) the variables C, $\sigma_{n'}(E_0, \theta)$ and B_i were determined by linear least-squares fitting to the spectrum. A further feature to improve the fit to the spectrum was that the function in equation (1) could be varied non-linearly in ΔE, constrained to minimize the residual of the fit. This resulted in improved fits as gauged from the reduced chi-squared values (χ_{vd}) which were typically in the range of between 1 and 3 for typically 500 and 1000 data points with <10 variables (i.e. the number of degrees of freedom, $vd \approx 490$–990). In addition, the spectrometer detection efficiency was calibrated against the He inelastic spectrum (Nickel *et al* 1989) and the spectra were individually corrected for this calibration. An energy loss spectrum with an example of such a fit is shown in figure 1.

(iii) It is clearly seen from equation (1) that a reliable unfolding fit depends on getting good FC factors. In the present case, a very careful survey of these was taken and we found that in all cases, small differences (from a few % to 20%) existed between various quoted values of $q_{n',v}$. Therefore, before proceeding with the measurements, we carried out numerical calculations of the vibrational wavefunctions of the ground and excited states using available potential energy (PE) curves for H_2. The following PE curves were used to obtain the vibrational wavefunctions $\chi_{n',v}(R)$. These are mostly compiled in the review by Sharp (1971). We used: for the $X\,^1\Sigma_g^+$ the theoretical PE curve of Kolos and Wolniewicz (1965), for the $B\,^1\Sigma_u^+$, $a\,^3\Sigma_g^+$ and $C\,^1\Pi_u$ states

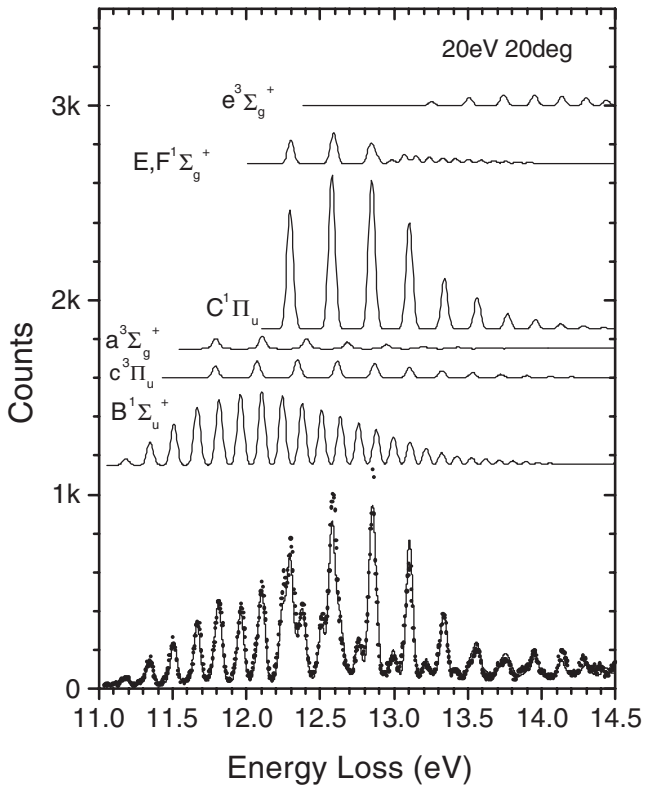

Figure 1. Experimental electron energy loss spectrum of H_2 (dots) taken at $E_0 = 20$ eV and $\theta = 20°$ with a fitted spectrum (curve) and showing the positions of the unfolded vibrational manifolds as a result of the fitting.

the PE curves of Kolos and Wolniewicz (1968), for the c $^3\Pi_u$ state the PE curve of Browne (1964), for the E, F $^1\Sigma_g^+$ state the PE curves of Kolos and Wolniewicz (1969) and for the e $^3\Sigma_g^+$ state the RKR potential (see Gilmore 1965) constructed by Sharp (1971) from the experimental results of Dieke (1958). The H_2 vibrational Schrödinger equation was then numerically solved with these PE curves using a numerical method based on finite differences. We started with the Schrödinger wave equation for the ground-state vth vibrational eigenfunction of the n'th electronic level $\chi_{n',v}(R)$:

$$-\frac{\hbar^2}{2m}\nabla^2\chi_{n',v}(R) + V_{n'}(R)\chi_{n',v}(R) = E\chi_{n',v}(R) \tag{4}$$

which was partitioned into a grid of $1 \ldots n \ldots N$ elements separated in R by ΔR yielding

$$-\frac{\hbar^2}{2m}\frac{\mathrm{d}^2}{\mathrm{d}R^2}\chi_{n',v}(R)\bigg|_{R=R_n} + V_{n'}(R_n)\chi_{n',v}(R_n) = E\chi_{n',v}(R_n). \tag{5}$$

We approximated the first term using the derivative finite-difference formula

$$-\frac{\hbar^2}{2m}\frac{\chi_{n',v}(R_{n-1}) - 2\chi_{n',v}(R_n) + \chi_{n',v}(R_{n+1})}{\Delta R^2} + V_{n'}(R_n)\chi_{n',v}(R_n) = E\chi_{n',v}(R_n) \tag{6}$$

and solved for $\chi_{n',v}(R_n)$ as

$$\chi_{n',v}(R_n) = -\frac{\hbar^2}{2m\Delta R^2}\frac{\chi_{n',v}(R_{n-1}) + \chi_{n',v}(R_{n+1})}{E - V_{n'}(R_n) - \frac{\hbar^2}{m\Delta R^2}}. \tag{7}$$

Table 1. Summary of excitation energies and FC factors for the vibrational components of the electronic states of H_2 which were unfolded from the electron energy loss spectra obtained in this work.

	B $^1\Sigma_g^+$		c $^3\Pi_u$		a $^3\Sigma_g^+$		C $^1\Pi_u$		E(F) $^1\Sigma_g^+$		e $^3\Sigma_u^+$	
v'	ΔE (eV)	$F(0, v')$	ΔE (eV)	$F(0, v')$	ΔE (eV)	$F(0, v')$	ΔE (eV)	$F(0, v')$	ΔE (eV)	$F(0, v')$	ΔE (eV)	$F(0, v')$
0	11.183	0.0086	11.789	0.1019	11.793	0.2085	12.295	0.1835	12.301	0.1690	13.253	0.0592
1	11.348	0.0295	12.072	0.1517	12.108	0.2563	12.578	0.2361	12.322	—	13.507	0.1244
2	11.508	0.0511	12.347	0.1633	12.405	0.2020	12.849	0.2301	12.470	—	13.742	0.1695
3	11.666	0.0733	12.615	0.1503	12.684	0.1345	13.103	0.1644	12.590	0.2288	13.950	0.1696
4	11.815	0.0828	12.868	0.1295	12.949	0.0820	13.341	0.0802	12.612	0.0010	14.137	0.1512
5	11.960	0.0891	13.104	0.0961	13.197	0.0483	13.562	0.0421	12.745	0.0012	14.301	0.1214
6	12.104	0.0915	13.323	0.0654	13.430	0.0279	13.768	0.0238	12.841	0.1382	14.438	0.0888
7	12.243	0.0871	13.529	0.0454	13.647	0.0163	13.957	0.0144	12.879	0.0500	14.538	0.0521
8	12.378	0.0818	13.723	0.0306	13.847	0.0095	14.129	0.0084	12.985	0.0285	14.612	0.0410
9	12.509	0.0723	13.899	0.0207	14.030	0.0057	14.283	0.0055	13.069	0.0684	14.662	0.0228
10	12.636	0.0620	14.059	0.0148	14.195	0.0034	14.418	0.0035	13.147	0.0583		
11	12.759	0.0532	14.202	0.0098	14.341	0.0021	14.531	0.0022	13.238	0.0480		
12	12.879	0.0445	14.325	0.0072	14.463	0.0013	14.621	0.0015	13.328	0.0416		
13	12.995	0.0364	14.432	0.0050	14.524	0.0008	14.680	0.0007	13.415	0.0381		
14	13.107	0.0290	14.521	0.0034	14.559	0.0005			13.502	0.0315		
15	13.217	0.0217	14.593	0.0027	14.623	0.0004			13.588	0.0264		
16	13.322	0.0154	14.646	0.0012	14.663	0.0003			13.673	0.0226		
17	13.424	0.0114	14.675	0.0008	14.691	0.0002			13.756	0.0191		
18	13.523	0.0095	14.689	0.0002					13.837	0.0160		
19	13.619	0.0079							13.917	0.0133		
20	13.712	0.0066										
21	13.803	0.0056										
22	13.892	0.0046										
23	13.978	0.0036										
24	14.055	0.0028										
25	14.123	0.0023										
26	14.192	0.0020										
27	14.267	0.0020										
28	14.344	0.0018										
29	14.425	0.0016										
30	14.491	0.0016										
31	14.509	0.0014										
32	14.558	0.0013										
33	14.594	0.0012										
34	14.602	0.0011										
35	14.634	0.0005										

Here $V_{n'}(R)$ is the inter-nuclear potential defining the PE curves for the n' electronic state as calculated by the above-mentioned authors, E is the energy level and m is the reduced mass. The numerical values of $V(R)$ were interpolated using a cubic-spline fit. Initially, a trial function for $\chi_{v=0}(R)$ was relaxed to converge into the ground state. The next $\chi_{n',v}(R)$ were obtained by repeating the relaxation, but constraining the state after each relaxation to be orthonormal to those $\chi_{n',v}(R)$ below it, by subtracting their overlap:

$$\chi_{n',v}(R) = \chi_{n',v}(R) - \sum_{s=0}^{v-1} \langle \chi_{n',v}(R), \chi_{n',s}(R) \rangle \chi_{n',s}(R) \tag{8}$$

and normalizing the wavefunction of this level relative to those below it:

$$\chi_{n',v}(R) = \frac{\chi_{n',v}(R)}{\langle \chi_{n',v}(R), \chi_{n',v}(R) \rangle}. \tag{9}$$

To ensure rapid convergence, the limits of our grid in R were constructed to terminate far away from the region of interest. The method was satisfactorily tested using a Morse potential. The resulting numerical vibrational eigenfunctions $\chi_{n',v,}(R)$ were used to calculate the FC integrals appropriately as

$$q_{n',v} = \left[\int_0^\infty \chi_{n',v}(R) \chi_{n'=1,v}(R) \mathrm{d}R \right]^2 \tag{10}$$

with the normalizing constraint that

$$\sum_v q_{n',v} = 1. \tag{11}$$

The $(E_{n',v})$ eigenvalues are then the expectation values of these wavefunctions for the E-operator from equation (4). Our energy values showed excellent agreement with those compiled by Sharp (1971).

The above-obtained FC factors control the accuracy of our spectral analysis, but they are also determined by the accuracy of the molecular PE curves which have to be accurate in the sub-1% region. The calculation of the molecular PE curves is checked by experimental data on the rotational inertia of the molecule, and is essentially insensitive to the fine structure of the electronic orbitals. However, small variations in the PE curves can be expected to result in a larger variation in our FC factors because of the sensitive and complicated dependence of $\chi_{n',v}(R)$ on $V_{n'}(R)$. We have not formulated an estimate of this factor, but we made the following effort to check its influence. To empirically check the theoretical FC factors, we took zero-angle energy loss spectra at $E_0 = 100$ eV for the $\Delta E = 11$–13.5 eV range i.e. predominantly the singlet state-excitations ($\mathrm{X}\ ^1\Sigma_g^+ \rightarrow \mathrm{B}\ ^1\Sigma_u^+$, $\mathrm{C}\ ^1\Pi_u$) since the dipole selection rule $g \not\Leftrightarrow g$ forbids the excitation of the $\mathrm{E, F}\ ^1\Sigma_g^+$ state from the $\mathrm{X}\ ^1\Sigma_g^+$ ground state (see Herzberg 1945). At this energy, the transmission of the electron analyser is also known to be constant across the spectrum. Hence careful fitting of the spectra should reveal differences between the theoretical and true FC factors. In figure 2, we show the comparison of our theoretical and the semi-empirically derived FC factors for the B and C states. As can be seen, there are significant differences between the two sets of FC factors. These are due to the accuracy in the evaluation of the overall FC integrals (see equation (10)). Surprisingly, however, using the theoretical (as opposed to our semi-empirical) FC factors does not bring about the expected large change in the overall intensity of the B and C states, but does affect the unfolding of the weaker states significantly. The accurate unfolding of the weaker features is therefore a limitation of the present spectrum-unfolding method. This is further commented on in section 3 when we discuss our results in comparison to our earlier measurements.

2.2. Experimental outline

In this experiment, the electron energy loss spectrometer was constructed with double-hemispherical energy selectors in both the gun and the analyser sections as has been detailed in Guo *et al* (2000). The spectrometer was housed in a vacuum chamber, which was pumped with a 12 inch diffusion pump. The base pressure of the vacuum chamber was 1×10^{-7} Torr. Both the gun and the analyser sections were baked to about 120 °C during the experiment to maintain the stable conditions necessary for taking electron energy loss spectra over long periods. To reduce the earth's magnetic field the vacuum chamber was shielded with two

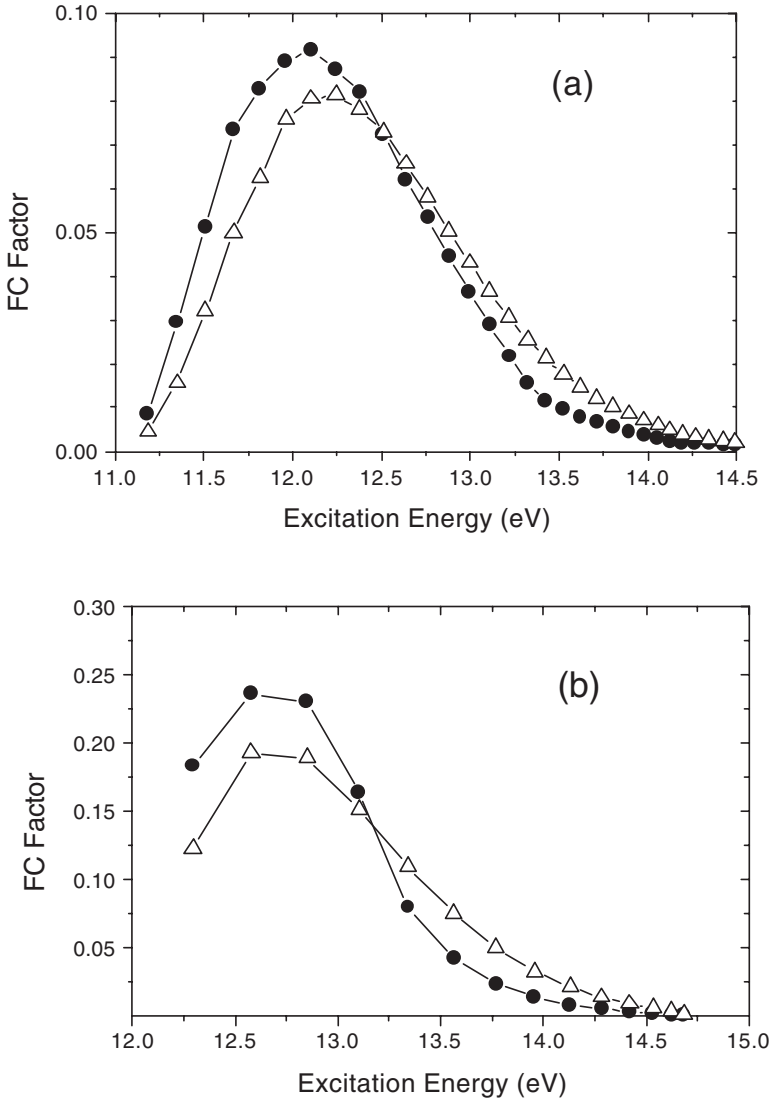

Figure 2. Comparison of present (filled circles) and previous (open triangles) FC factors for the (a) B $^1\Sigma_u^+$ and (b) C $^1\Pi_u$ states of H_2. See text for discussion.

double-layered high-permeability, low-field μ-metal and high-field, low-permeability double μ-metal shield combinations. The double-layer shields were further de-magnetized using a 100A-bearing coil powered by an AC welding power-supply which was slowly turned on and off by a variac transformer. The coil was formed in between the μ-metal layers and its use enabled the magnetic field in the chamber to be reduced to 1–2 mG. As mentioned, an important feature of this spectrometer is the absence of 'wings' in the instrumental profile, often seen in spectrometers with single-hemispherical analysers. This characteristic enabled us to obtain an accurate line profile for this instrument and thus more accurately unfold the molecular spectra. The spectrometer operated at an energy resolution of 25–40 meV (FWHM) with an electron current ranging from 3 to 20 nA. It could observe scattered electrons at scattering

angles up to 130°. Contact potential measurements using the He^- $1s2s^2$ resonance enabled us to calibrate our incident energy to well within ±0.05 eV.

This apparatus was computer-controlled to enable efficient data acquisition. The computer processed the multi-channel scaling measurement of the energy loss scan as well as controlling the scattering angle positioning. It monitored the pressure behind the gas line and modulated the gas beam via a thin molybdenum beam flag to determine the experimental background contribution to the elastic (≈20% at small θ to ≈2% at large θ) and inelastic (<3%) features. Analysis of the measured spectra was done off-line.

The spectra were taken with the elastic (zero energy loss) peak followed by a scan from 11 to 14.5 eV. Step size was typically 4 or 5 meV. This enabled us to obtain relative DCSs after normalization to the elastic H_2 DCSs of Khakoo and Trajmar (1986a) at each E_0. Here we assume that the analyser response did not vary during the measurements. This was ensured by leaving the analyser settings untouched (except for small adjustments to the hemispheres) and was checked by repeating measurements. Finally, at θ of 90° and 60° the spectra were normalized absolutely by determining the analyser response using He at $E_0 = 30.6$ eV as detailed in Nickel *et al* (1989).

3. Results and discussion of results

Table 2 summarizes the DCSs and their associated uncertainties. The uncertainties include:

(a) the error contribution of the elastic cross-section standard (Khakoo and Trajmar 1986a) of 13%, 13% and 12% at E_0 values of 17.5, 20 and 30 eV;
(b) the normalization of the inelastic cross-sections to the elastic cross-sections, i.e. the determination of instrumental transmission, which varied from 4% to 7%; and
(c) errors induced in unfolding the features from the energy loss spectra (an estimated 10% for the FC factors, a factor of 2–3% on the response of the analyser across the spectrum and statistical errors).

3.1. $E_0 = 17.5$ *eV*

At $E_0 = 17.5$ eV (figures 3(a)–(f)), we can only compare with the multi-channel Schwinger calculations of Lima *et al* (1988) for the c $^3\Pi_u$ and a $^3\Sigma_g^+$ states and the distorted wave calculations of Rescigno *et al* (1976) for the a $^3\Sigma_g^+$ state. We note that both theories give reasonable shapes, but the multi-channel Schwinger does very well in the case of the a $^3\Sigma_g^+$ state whereas the distorted wave is about a factor of 5 too high (figure 3(c)). For the c $^3\Pi_u$ state (figure 3(b)), the multi-channel Schwinger still gives a reasonable quantitative result, but is a factor of 10 too high. This is a surprising result: one would expect the accuracy for both the X $^1\Sigma_g^+ \rightarrow$ c $^3\Pi_u$ and a $^3\Sigma_g^+$ forbidden transitions to be similar. There are no other published results for these states at $E_0 = 17.5$ eV. We note the relatively flat angular distribution of the c $^3\Pi_u$ and e $^3\Sigma_u^+$ DCSs at this energy. Both the B $^1\Sigma_u^+$, C $^1\Pi_u$ and the E, F $^1\Sigma_g^+$ state DCSs show typical forward-peaked DCSs characteristic of dipole-allowed transitions, but the E, F $^1\Sigma_g^+$ shows some structure at around $\theta = 90°$.

3.2. $E_0 = 20$ *eV*

At $E_0 = 20$ eV, in figure 4(a) we see excellent quantitative agreement between the present DCSs for the B $^1\Sigma_u^+$, our earlier measurements (Khakoo and Trajmar 1986b) and the distorted

Table 2. Summary of differential electron impact excitation cross-sections for excitation of the $B\,^1\Sigma_u^+$, $c\,^3\Pi_u$, $a\,^3\Sigma_g^-$, $C\,^1\Pi_u$, E, $F\,^1\Sigma_g^+$ and $e\,^3\Sigma_u$ states of H_2 with corresponding uncertainties (see section 3 (a)–(c)). (a) $E_0 = 17.5$ eV; (b) $E_0 = 20$ eV and (c) $E_0 = 30$ eV. (Units: $\times 10^{-18}$ cm^2/sr.)

Angle	$B\,^1\Sigma_g^+$		$c\,^3\Pi_u$		$a\,^3\Sigma_g^+$		$C\,^1\Pi_u$		$E(F)\,^1\Sigma_g^+$		$e\,^3\Sigma_u^+$	
(deg)	State	Error	State	Error	State	Error	State	Error	State	Error	State	Error
(a)												
10	6.74	1.31	1.33	0.26	1.39	0.27	3.430	0.670	1.570	0.310	0.090	0.023
15	5.35	1.04	1.31	0.29	0.95	0.20	2.580	0.550	1.680	0.370	0.073	0.027
20	3.28	0.73	1.42	0.35	1.45	0.35	2.570	0.700	1.340	0.330	0.120	0.033
30	3.40	0.74	1.41	0.33	0.93	0.20	1.840	0.450	0.550	0.140	0.130	0.028
40	1.99	0.41	1.49	0.33	0.76	0.18	1.250	0.302	0.360	0.095	0.060	0.015
50	1.53	0.32	1.34	0.28	0.78	0.18	0.740	0.170	0.190	0.043	0.060	0.016
60	1.13	0.21	1.12	0.21	0.47	0.09	0.660	0.140	0.220	0.048	0.050	0.013
70	1.25	0.24	1.02	0.30	0.53	0.14	0.590	0.130	0.130	0.036	0.080	0.023
80	1.06	0.22	0.76	0.18	0.48	0.13	0.470	0.107	0.220	0.060	0.080	0.022
90	0.95	0.20	0.69	0.16	0.43	0.10	0.390	0.085	0.200	0.050	0.130	0.034
100	1.01	0.23	0.83	0.23	0.47	0.14	0.370	0.084	0.260	0.078	0.100	0.026
110	0.73	0.17	0.57	0.15	0.38	0.10	0.404	0.103	0.090	0.030	0.072	0.023
120	0.87	0.17	0.48	0.12	0.42	0.12	0.351	0.100	0.064	0.019	0.079	0.02
130	0.97	0.20	0.56	0.15	0.45	0.13	0.476	0.121	0.120	0.033	0.089	0.027
ICS	17.01	3.51	10.9	2.58	6.99	1.69	8.76	2.046	3.10	0.729	1.08	0.296
(b)												
5	34.80	6.47	4.29	0.92	1.62	0.36	24.190	4.500	2.440	0.527	0.230	0.08
10	23.22	4.32	3.20	0.81	1.89	0.49	17.150	3.190	2.040	0.490	1.050	0.25
15	19.41	3.61	3.33	0.73	1.62	0.35	15.820	2.940	1.100	0.260	1.550	0.37
20	15.25	2.76	3.79	0.84	1.72	0.36	11.960	2.269	0.850	0.240	1.450	0.35
30	6.12	1.17	2.86	0.71	1.37	0.36	4.510	0.890	0.300	0.075	0.300	0.08
40	2.96	0.57	2.42	0.54	1.03	0.25	1.950	0.380	0.100	0.041	0.097	0.03
50	2.24	0.45	2.41	0.55	1.00	0.25	1.480	0.310	0.185	0.068	0.130	0.03
60	1.58	0.33	2.05	0.50	0.68	0.17	0.910	0.200	0.550	0.150	0.110	0.03
70	1.83	0.37	2.28	0.54	0.65	0.17	1.060	0.219	0.500	0.130	0.130	0.04
80	1.61	0.29	1.68	0.40	0.84	0.25	0.830	0.190	0.530	0.118	0.080	0.02
90	1.11	0.23	1.61	0.33	0.79	0.19	0.530	0.128	0.450	0.127	0.110	0.03
100	0.89	0.18	1.74	0.35	0.54	0.14	0.460	0.103	0.500	0.113	0.240	0.065
110	0.55	0.12	1.62	0.36	0.57	0.14	0.450	0.107	0.250	0.063	0.220	0.067
120	0.45	0.09	1.54	0.35	0.62	0.14	0.480	0.108	0.150	0.039	0.170	0.04
130	0.40	0.10	1.76	0.42	0.70	0.17	0.530	0.108	0.200	0.063	0.130	0.0438
ICS	27.68	5.19	24.89	5.72	10.11	2.47	19.84	3.80	4.68	1.18	2.52	0.70
(c)												
5	97.85	18.18	6.56	1.44	2.42	0.51	75.780	14.080	10.600	1.990	1.920	0.37
10	72.33	13.44	3.75	0.93	1.24	0.28	56.290	10.460	8.910	2.200	1.920	0.4
15	35.66	6.37	3.63	0.79	0.77	0.20	32.350	5.860	2.220	0.520	1.100	0.25
20	18.81	3.43	2.42	0.59	0.55	0.13	15.960	3.400	0.590	0.158	0.670	0.17
30	6.43	1.18	1.75	0.39	0.32	0.08	5.080	0.970	0.330	0.100	0.230	0.06
40	2.12	0.42	1.10	0.29	0.13	0.03	1.510	0.330	0.150	0.062	0.097	0.033
50	1.07	0.21	1.16	0.29	0.08	0.02	0.930	0.190	0.082	0.035	0.060	0.02
60	1.00	0.17	0.70	0.18	0.07	0.02	0.660	0.160	0.100	0.046	0.090	0.028
70	0.78	0.15	0.71	0.19	0.05	0.01	0.450	0.100	0.200	0.064	0.050	0.016
80	0.60	0.11	0.50	0.14	0.07	0.02	0.340	0.073	0.300	0.100	0.070	0.02
90	0.49	0.09	0.42	0.10	0.11	0.03	0.300	0.070	0.190	0.060	0.060	0.0149
100	0.32	0.07	0.33	0.09	0.11	0.03	0.260	0.060	0.190	0.048	0.060	0.0168
110	0.22	0.04	0.24	0.08	0.10	0.03	0.210	0.050	0.180	0.044	0.050	0.0147
120	0.21	0.04	0.14	0.04	0.09	0.03	0.200	0.048	0.210	0.070	0.020	0.0055
130	0.13	0.03	0.09	0.02	0.15	0.03	0.180	0.044	0.140	0.046	0.010	0.004
ICS	31.79	5.87	7.96	1.88	1.86	0.56	25.60	4.82	4.02	0.92	1.32	0.29

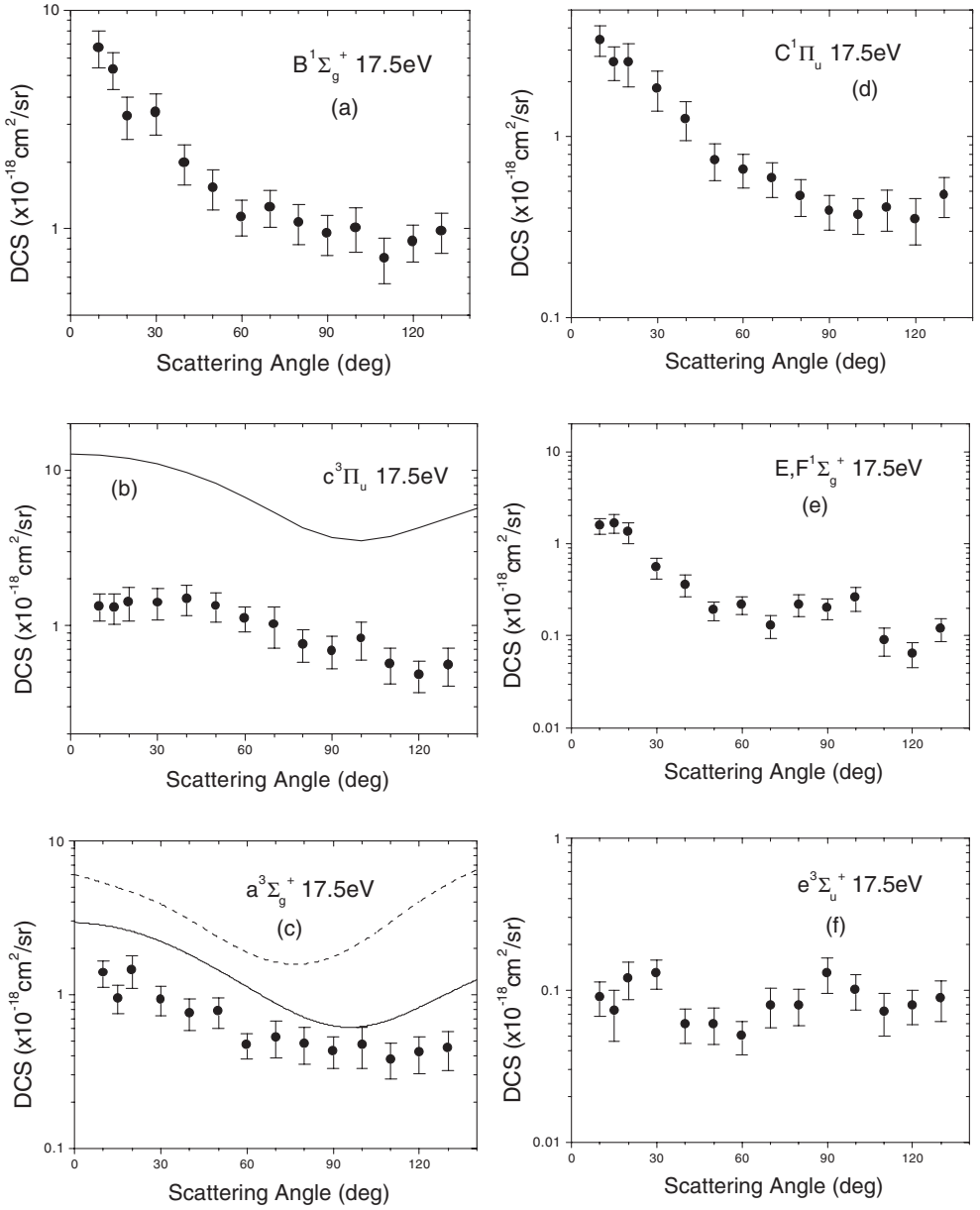

Figure 3. DCSs for the (a) B $^1\Sigma_u^+$, (b) c $^3\Pi_u$, (c) a $^3\Sigma_g^+$, (d) C $^1\Pi_u$, (e) E, F $^1\Sigma_g^+$ and (f) e $^3\Sigma_u$ states of H_2 taken at $E_0 = 17.5$ eV and compared with existing theoretical and experimental work. Legend: ● present work with error bars; —— Lima *et al* (1988) interpolated $E_0 = 16$ and 18 eV results; – – – Rescigno *et al* (1976).

wave calculations of Fliflet and McKoy (1980). The measurements of Srivastava and Jensen (1977) are in reasonable agreement with the present DCSs. The *R*-matrix results of Branchett *et al* (1991), while in reasonable average quantitative agreement, do not give the correct shape. This is perhaps a considerably higher E_0 value than is the range of applicability of close-coupling-type calculations.

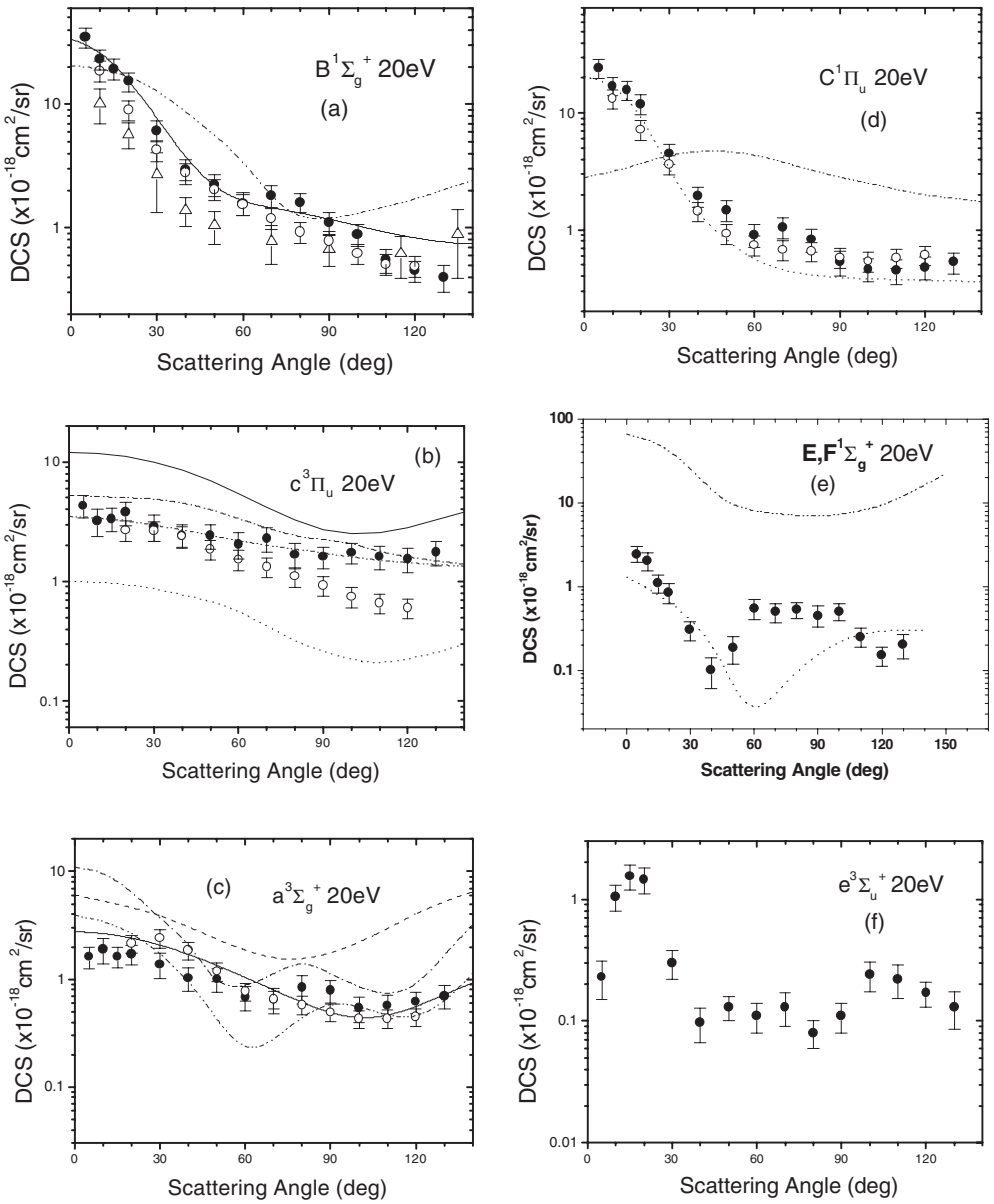

Figure 4. DCSs for the (a) B $^1\Sigma_u^+$, (b) c $^3\Pi_u$, (c) a $^3\Sigma_g^+$, (d) C $^1\Pi_u$, (e) E, F $^1\Sigma_g^+$ and (f) e $^3\Sigma_u$ states of H_2 taken at $E_0 = 20$ eV and compared with existing theoretical and experimental work. Legend same as figure 3 except: experiments: △, Srivastava and Jensen (1977); ○, Khakoo and Trajmar (1986b); theories: – – – Rescigno *et al* (1976); —— Fliflet and McKoy (1980, B $^1\Sigma_u^+$ state); · · · · · · Mu-Tao *et al* (1982); —— Lima *et al* (1988, a $^3\Sigma_g^+$ and c $^3\Pi_u$ states); — · — Parker *et al* (1991); and — · · — Branchett *et al* (1991).

In contrast, the same R-matrix results for the c $^3\Pi_u$ state (figure 4(b)) at this E_0 show excellent agreement with the present DCSs. We note that our earlier DCSs (Khakoo and Trajmar 1986b) are in good agreement with the present results at small θ, but are a factor of 1.5 below at larger θ. The complex Kohn DCSs of Parker *et al* (1991) are a little higher than the

present results, but nevertheless are in good agreement. The distorted wave results of Mu-Tao *et al* (1982) and those of Lima *et al* (1988) are not in agreement with the experimental DCSs.

For the a $^3\Sigma_g^+$ DCSs (figure 4(c)) we find very good agreement between the present and our earlier DCSs. Best agreement with theory is found with the multi-channel Schwinger DCSs of Lima *et al* (1988), but disagreement with the other theories (Parker *et al* 1991, Mu-Tao *et al* 1982, Branchett *et al* 1991) which show disagreement between each other as far as angular shapes are concerned.

For the C $^1\Pi_u$ state DCSs (figure 4(d)) the present results are in very good agreement with our earlier DCSs (Khakoo and Trajmar 1986b). The calculations of Mu-Tao *et al* (1982) are in very good agreement with the experimental values. However, the *R*-matrix DCSs of Branchett *et al* (1991) show severe disagreement, producing a shape that is physically unrealistic for a dipole-allowed transition. This suggests a problem in the present *R*-matrix code and because it is a close-coupling calculation, it means that the other channels may also be affected.

The DCSs for the E, F $^1\Sigma_g^+$ state (figure 4(e)) show a similar situation as for the C $^1\Pi_u$ state. We see very good agreement with the distorted wave results of Mu-Tao *et al* (1982), which gives good shape agreement with the present results, showing the strong dip in the E, F $^1\Sigma_g^+$ DCSs at intermediate θ.

Finally, the e $^3\Sigma_u^+$ state DCSs (figure 4(f)) show a very complicated angular behaviour with a marked peak at small scattering angles over a very small θ range of 10°–30°.

3.3. $E_0 = 30$ *eV*

At this energy, for the B $^1\Sigma_u^+$ state (figure 5(a)), agreement between all experiments is excellent. We note that the only theoretical DCSs of Fliflet and McKoy (1980) are also in excellent qualitative agreement, but are significantly larger than the present measurements by about 40%.

For the c $^3\Pi_u$ state DCSs (figure 5(b)) there is disagreement between the present DCSs and those of our earlier measurements (Khakoo and Trajmar 1986b) in the angular interval of $40° < \theta < 110°$. This is similar to the situation observed at $E_0 = 20$ eV (figure 4(b)). Comparison with the theoretical DCSs (complex Kohn method) of Parker *et al* (1991) and (multi-channel Schwinger) of Lima *et al* (1988) shows disagreement overall. We note, however, that the results of Parker *et al* show a decreasing trend similar to that observed in the present DCSs.

For the a $^3\Sigma_g^+$ (figure 5(c)), very good shape agreement is observed between the present and earlier measurements and also with the complex Kohn method DCSs of Parker *et al*. However, the present DCSs are lower than the earlier values. The DCSs of Lima *et al* (1988) are in disagreement with our present results.

For the C $^1\Pi_u$ state DCSs (figure 5(d)) the present and earlier measurements (Khakoo and Trajmar 1986b) are in very good agreement except at small θ, where the present DCSs are higher than the earlier values.

For the E, F $^1\Sigma_g^+$ state (figure 5(e)) there are no theoretical DCSs to compare with, but we note that the angular distribution is very similar to that observed at $E_0 = 20$ eV.

For the e $^3\Sigma_u^+$ state DCSs (figure 5(f)) the very complicated angular behaviour observed at $E_0 = 20$ eV is not observed, but rather an angular distribution that is forward peaked, with a flat region around $\theta = 90°$.

3.4. Overall

The overall picture as far as comparison between the present and earlier values is concerned is mixed. The agreement between experiments is good considering the fact that the new

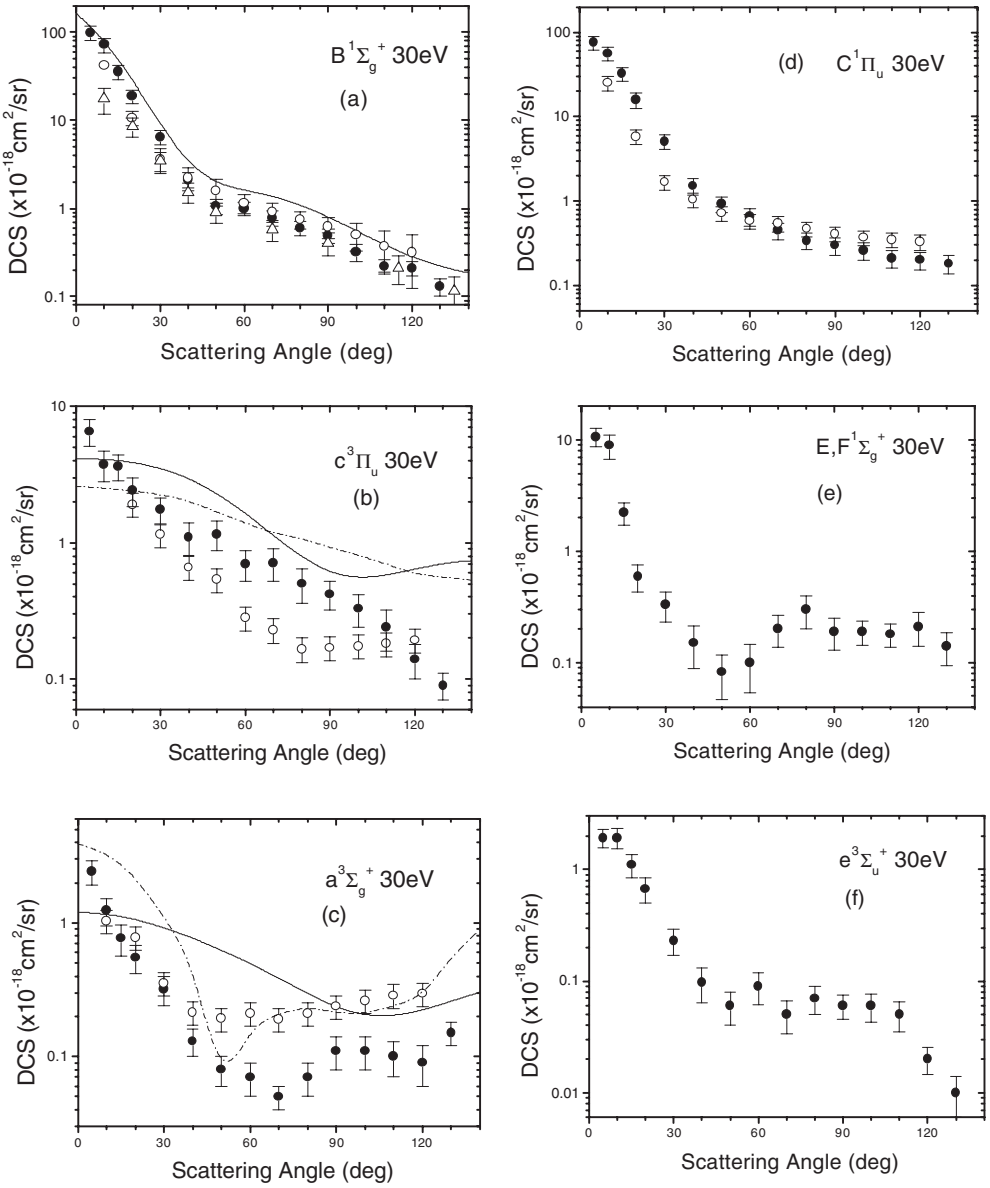

Figure 5. As figure 4, but for $E_0 = 30$ eV.

DCSs were obtained with (slightly) different FC factors than those used earlier (Khakoo and Trajmar 1986b). We note that regions where increased disagreements are observed between the measurements is largely due to the influence of the line profile in the unfolding algorithm, especially for the c $^3\Pi_u$ and a $^3\Sigma_g^+$ which are dominated by the dipole-allowed B $^1\Sigma_u^+$ and C $^1\Pi_u$ states. The wings in the line profiles from the earlier results (Khakoo and Trajmar 1986b) taken with a single-hemispherical spectrometer, coupled with the fact that only single Gaussians were used to describe the earlier instrument's line profile, probably affected the unfolding results by taking intensity away from these weaker features or sometimes adding to it, depending on the

intensities of the dipole-forbidden features relative to the dipole-allowed features. Comparison with theoretical values is also mixed. The only consistently good agreement is observed with the distorted wave results of Fliflet and McKoy (1980) for the B $^1\Sigma_u^+$ state. Otherwise, no theory is consistently in any agreement for all the states' DCSs observed here. We again note that although new FC factors calculated by us were used, these did not cause significant change in the unfolded DCSs.

4. Conclusions

We present new, improved, normalized DCSs taken for the electron impact excitation of the low-lying bound states of H_2. Reasonable-to-good agreement is observed with the earlier DCSs taken by us (Khakoo and Trajmar 1986b). However, we still find severe disagreements with existing theoretical models. It is hoped that the present experimental results instigate new and more reliable calculations for these important transitions for this fundamental molecular target, for which (at present) there remains considerable work to be done in the form of both theoretical and experimental research.

Acknowledgments

This work was funded by a grant from NASA Planetary Astronomy and Atmospheres Program under grant NRA 95-OSS-05 and by the National Science Foundation under grants RUI-PHY 9511549 and RUI-PHY 0096808.

References

Branchett S E, Tennyson J and Morgan L A 1990 *J. Phys. B: At. Mol. Opt. Phys.* **23** 4625
Branchett S E, Tennyson J and Morgan L A 1991 *J. Phys. B: At. Mol. Opt. Phys.* **24** 3479
Browne J C 1964 *J. Chem. Phys.* **40** 43
Burke P G and Robb W D 1975 *Adv. At. Mol. Phys.* **11** 144
Dieke G H 1958 *J. Mol. Spectrosc.* **2** 494
Fliflet A W and McKoy V 1980 *Phys. Rev.* A **21** 1863
Gilmore F 1965 *J. Quant. Spectrosc. Radiat. Transfer* **5** 369
Guo X, Mathews D J, Mikaelian G, Khakoo M A, Crowe A, Kanik I, Trajmar S, Zeman V, Bartschat K and Fontes C J 2000 *J. Phys. B: At. Mol. Opt. Phys.* **33** 1895
Hall R I and Andric L 1984 *J. Phys. B: At. Mol. Phys.* **17** 3815
Herzberg G 1945 *Molecular Spectra and Molecular Structure. I: Spectra of Diatomic Molecules* (New York: Van Nostrand-Reinhold)
Khakoo M A and Segura J 1994 *J. Phys. B: At. Mol. Opt. Phys.* **27** 2355
Khakoo M A and Trajmar S 1986a *Phys. Rev.* A **34** 138
Khakoo M A and Trajmar S 1986b *Phys. Rev.* A **34** 146
Khakoo M A and Trajmar S 1987 *Phys. Rev.* A **35** 2832
Kolos W and Wolniewicz L 1965 *J. Chem. Phys.* **43** 2429
Kolos W and Wolniewicz L 1968 *J. Chem. Phys.* **48** 3672
Kolos W and Wolniewicz L 1969 *J. Chem. Phys.* **50** 3228
Lima M A P, Gibson T L, McKoy V and Huo W M 1988 *Phys. Rev.* A **38** 4527
Mu-Tao L, Lucchese R R and McKoy V 1982 *Phys. Rev.* A **26** 3240
Nickel J, Zetner P W, Shen G and Trajmar S 1989 *J. Phys. E: Sci. Instrum.* **22** 730
Nishimura H and Danjo A 1986 *J. Phys. Soc. Japan* **55** 3031
Parker S D, McCurdy C W, Rescigno T N and Lengsfield B H III 1991 *Phys. Rev.* A **43** 3514
Pinnaduwage L A and Christophorou L G 1993 *Phys. Rev. Lett.* **70** 754
Pinnaduwage L A and Christophorou L G 1994 *J. Appl. Phys.* **76** 46

Rescigno T N, McCurdy C W, McKoy V and Bender C F 1976 *Phys. Rev.* A **13** 216
Sharp T E 1971 *At. Data* **2** 119–69
Shemansky D E, Ajello J M and Hall D T 1985 *Astrophys. J.* **296** 765
Srivastava S and Jensen S 1977 *J. Phys. B: At. Mol. Phys.* **10** 3341 (renormalized by Trajmar S, Register D F and Chutjian A 1983 *Phys. Rep.* **97** 219)
Trajmar S, Cartwright D C, Rice J K, Brinkmann R T and Kupperman A 1968 *J. Chem. Phys.* **49** 5464
Weingartshofer A, Ehrhardt H, Hermann V and Linder F 1970 *Phys. Rev.* A **2** 294